AGU PUBLICATIONS

Geophysical Research Letters

RESEARCH LETTER
10.1002/2013GL059086

Key Points:
- Measurements of MODIS FRP have an uncertainty of 26.6% at the 1 sigma level
- Uncertainties in MODIS FRP are driven by the fire location within the PSF
- Uncertainties in MODIS FRP do not depend on scan angle

Correspondence to:
P. H. Freeborn,
patrick.freeborn@sdstate.edu

Citation:
Freeborn, P. H., M. J. Wooster, D. P. Roy, and M. A. Cochrane (2014), Quantification of MODIS fire radiative power (FRP) measurement uncertainty for use in satellite-based active fire characterization and biomass burning estimation, *Geophys. Res. Lett.*, *41*, 1988–1994, doi:10.1002/2013GL059086.

Received 18 DEC 2013
Accepted 13 FEB 2014
Accepted article online 18 FEB 2014
Published online 28 MAR 2014

Quantification of MODIS fire radiative power (FRP) measurement uncertainty for use in satellite-based active fire characterization and biomass burning estimation

Patrick H. Freeborn[1], Martin J. Wooster[2,3], David P. Roy[1], and Mark A. Cochrane[1]

[1]Geographic Information Science Center of Excellence, South Dakota State University, Brookings, South Dakota, USA, [2]Earth and Environmental Dynamics Research Group, Department of Geography, King's College London, London, UK, [3]NERC National Centre for Earth Observation, UK

Abstract Satellite measurements of fire radiative power (FRP) are increasingly used to estimate the contribution of biomass burning to local and global carbon budgets. Without an associated uncertainty, however, FRP-based biomass burning estimates cannot be confidently compared across space and time, or against estimates derived from alternative methodologies. This work addresses this issue and quantifies the precision of Moderate Resolution Imaging Spectroradiometer (MODIS) measurements of FRP by collecting duplicate, off-nadir, overlapping observations of the same fires. Differences in the per-pixel FRP measured near-simultaneously in consecutive MODIS scans are approximately normally distributed with a standard deviation (σ_η) of 26.6%. Simulations demonstrate that this uncertainty decreases to less than ~5% (at ±1 σ_η) for aggregations larger than ~50 MODIS active fire pixels. Although FRP uncertainties limit the confidence in flux estimates on a per-pixel basis, the sensitivity of biomass burning estimates to FRP uncertainties can be mitigated by conducting inventories at coarser spatiotemporal resolutions.

1. Introduction

Quantifying fuel consumption and trace gas and aerosol emissions from biomass burning is fundamental to understanding the carbon cycle, terrestrial-atmosphere interactions, and climate change [*Bowman et al.*, 2009]. Traditionally, fuel consumption has been estimated as the product of the fire-affected area (units: m^2), the pre-burn fuel load (kg m^{-2}), and combustion completeness (unitless: 0–1) [*Seiler and Crutzen*, 1980]. Alternatively, *Kaufman et al.* [1996] proposed that the rate of emission of fire radiative energy could be used to indicate the rate of combustion. Since then, measurements of fire radiative power (FRP) from polar-orbiting sensors have been used to characterize active fire (AF) properties [e.g., *Wooster and Zhang*, 2004; *Smith and Wooster*, 2005; *Ichoku et al.*, 2008], to quantify biomass consumption and trace gas and aerosol production [e.g., *Ellicott et al.*, 2009; *Vermote et al.*, 2009; *Kaiser et al.*, 2012], and to estimate smoke plume heights [*Mazzoni et al.*, 2007; *Val Martin et al.*, 2010]. Although such applications require reliable measurements of FRP, comparisons of concurrent and collocated measurements of FRP from independent Earth observing sensors have shown large variability [e.g., *Wooster et al.*, 2003; *Roberts and Wooster*, 2008; *Xu et al.*, 2010; *Schroeder et al.*, 2010]. Furthermore, without an associated uncertainty, pyrogenic parameters derived from FRP cannot be confidently compared across space and time, or against estimates derived from traditional bottom-up approaches. As of yet, however, a formal study of the uncertainty in satellite measurements of FRP has not been conducted.

In this work, without a true FRP reference, we forego an accuracy assessment and instead quantify the precision (or repeatability) of Moderate Resolution Imaging Spectroradiometer (MODIS) measurements of FRP. We exploit an off-nadir sampling artifact, referred to as the "bow-tie effect" [*Wolfe et al.*, 2002], to collect near-simultaneous, overlapping MODIS observations of the same fire in consecutive scans. The percent difference in FRP between the first and second scans is used to gauge the uncertainty in MODIS measurements of FRP. We decompose measurement uncertainties into contributions from the fire pixel and the background window and examine the impacts of the fire's location relative to the MODIS point spread function (PSF). Finally, we offer a model to characterize measurement uncertainties in the sum of FRP for spatial and temporal aggregations of MODIS active fire pixels.

2. Background

2.1. Data Sets

Information about the timing, location, and radiative characteristics of MODIS active fire pixels is stored in a variety of formats [*Giglio*, 2013]. Here we use the Collection 5 Level 2 Fire Products (abbreviated MOD14 for Terra and MYD14 for Aqua) since these data sets provide the image and geographic coordinates, fire pixel and mean background brightness temperatures, and FRP for each individual 1 km AF pixel detected by MODIS. The MOD14/MYD14 files are available for download from NASA's Earth Observing System Clearing House Reverb client (http://reverb.echo.nasa.gov/reverb/). We analyze 10 years (2003–2012) of global data, consisting of 288 files per day for each of the MOD14 and MYD14 fire products.

2.2. MODIS Fire Radiative Power

FRP values (MW) stored in the Collection 5 MODIS fire product suite are calculated using the equation originally formulated by *Kaufman et al*. [1998] and amended by *Giglio* [2013] to account for variations in pixel size across the swath:

$$FRP = A_s \beta \left(T_f^8 - T_b^8\right) \quad (1)$$

where T_f is the 4 μm brightness temperature of the fire pixel, T_b is the mean 4 μm brightness temperature of the background window, A_s is the nominal MODIS pixel area evaluated at the scan angle, or sample number, s, and the coefficient $\beta = 4.34 \times 10^{-19}\,\mathrm{Wm^{-2}K^{-8}}$ is specific to the MODIS 4 μm spectral response. Although T_b is representative of a window that expands until at least 25% of the surrounding pixels are identified as valid cloud-free land pixels that are also not fire pixels [*Giglio et al*., 2003], it is still possible for T_b to be influenced by hot spots in the background window but not recognized by the MODIS active fire detection algorithm.

2.3. MODIS Sensing Geometry

MODIS acquires 4 μm images of the Earth's surface at a nominal 1 km spatial resolution at nadir using a scan mirror to reflect thermal radiance onto linear arrays of 10 detectors aligned on the focal plane in the along-track direction [*Barnes et al*., 1998]. Coverage in the N-S direction is achieved through forward motion of the satellite, and coverage in the E-W direction is achieved by rotating the scan mirror across a 110° Earth field of view (±55° off-nadir) in 0.451 s, collecting a 1 km sample every 333 μs [*Wolfe et al*., 2002]. A single MODIS scan is thus composed of 10 image lines in the along-track direction and 1354 samples (pixels) in the along-scan direction.

Whereas the MODIS point spread function (PSF) is nearly rectangular in the along-track direction, the motion of a pixel's instantaneous geometric field of view across the Earth's surface during the 333 μs sample results in a triangular PSF in the along-scan direction [*Nishihama et al*., 1997; *Barnes et al*., 1998]. This sampling scheme also results in 50% overlap in the ground area subtended by adjacent along-scan pixels [*Nishihama et al*., 1997]. Therefore, unless a fire is oriented perfectly along the MODIS pixel centerline, a fire will always be sensed by two adjacent along-scan pixels, and the fractional allocation of thermal radiance into adjacent along-scan pixels will depend on the location of the fire within the PSFs [*Schroeder et al*., 2010]. The fortuitous alignment of a fire within the MODIS ground footprint affects the measurement of pixel brightness temperatures, influences whether an AF pixel is detected or not, and ultimately impacts the retrieval of FRP [*Schroeder et al*., 2010].

The area subtended by a MODIS pixel (i.e., A_s) increases as a function of scan angle due to increased line-of-sight distances and Earth curvature [*Wolfe et al*., 2002]. As a consequence, substantial scan-to-scan overlap (>10%) in the along-track direction begins above scan angles of 24° where ground locations are sensed twice within ~1.48 s [see Fig. 4 in *Wolfe et al*., 2002]. When an AF pixel is detected at the same scan angle on the leading and trailing edges of consecutive scans, the FRP emitted from the same thermal anomaly is measured twice using different detectors with overlapping ground footprints.

3. Methods

Two sets of duplicate AF pixels detected in consecutive scans were extracted from the MOD14 and MYD14 fire products. In the first set, solitary AF pixels (i.e., one AF pixel per scan) were detected in consecutive scans at the same scan angle with at least one image line between each isolated AF pixel. In the second set, clusters

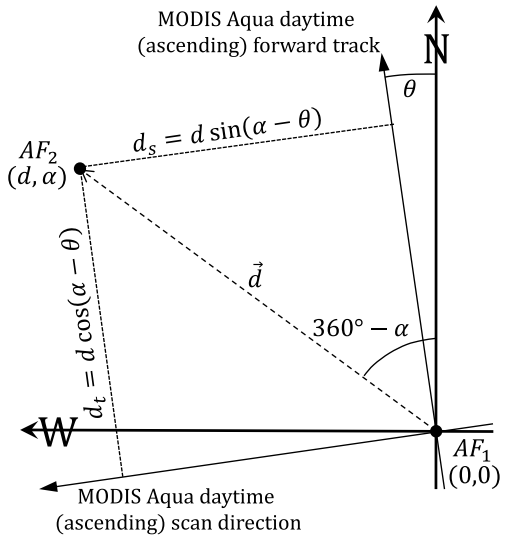

Figure 1. Example of a vector drawn from the center of a MODIS active fire (AF) pixel detected in the first scan (AF_1) to the center of an overlapping AF pixel detected in the second scan (AF_2). This geometry is specific to the Aqua daytime (ascending) node with an orbital inclination of $\theta = 8.2°$ west of true north.

of two contiguous AF pixels (i.e., two spatially adjacent AF pixels in either the along-scan or along-track direction) were detected in consecutive scans at the same scan angle, also with at least one image line between each cluster. For both sets, no other AF pixels were detected within the background windows.

3.1. Solitary Active Fire Pixels

For overlapping solitary AF pixels, the FRP measured in the first and second scans (FRP_1 and FRP_2, respectively) were used to calculate the percent difference in FRP, η, as follows:

$$\eta = 100\% \times \frac{\Delta FRP}{\overline{FRP}} \tag{2}$$

where ΔFRP is the absolute scan-to-scan difference in FRP ($\Delta FRP = FRP_1 - FRP_2$), and $\overline{FRP}$ is the average of FRP_1 and FRP_2. We calculate η based on $\overline{FRP}$ since neither FRP_1 nor FRP_2 can be considered the true value, and we use the standard deviation of η, σ_η (in percent), as an indicator of precision.

According to equation (1), ΔFRP can be attributed to scan-to-scan differences in T_f and/or T_b. Substituting equation (1) into equation (2) allows η to be decomposed into the following:

$$\eta = 100\% \times \left[\frac{A_s\beta\left(T_{f1}^8 - T_{f2}^8\right)}{\overline{FRP}} - \frac{A_s\beta\left(T_{b1}^8 - T_{b2}^8\right)}{\overline{FRP}}\right] \tag{3}$$

$$\eta = \eta_f - \eta_b \tag{4}$$

where T_{f1}, T_{f2}, T_{b1}, and T_{b2} are the fire pixel and mean background brightness temperatures measured in the first and second scans, respectively, and η_f and η_b are the contributions to η from the fire pixel and the background window, respectively.

Displacements in overlapping PSFs were determined by constructing a vector between the centers of the AF pixels detected in the first and second scans. This vector is described by distance (d) and azimuth (α). Figure 1 illustrates that d can be decomposed into the along-scan and along-track components (d_s and d_t) by taking into account the 98.2° orbital inclination of Aqua and Terra [*Wolfe et al.*, 2002]. Further normalizing d_s and d_t by the along-scan and along-track pixel dimensions, ΔS_s and ΔT_s, respectively, yields the relative displacements $\hat{d}_s$ and $\hat{d}_t$:

$$\hat{d}_s = \frac{d_s}{\Delta S_s} = \frac{|d|\ sin\ (\alpha-\theta)}{\Delta S_s} \tag{5}$$

$$\hat{d}_t = \frac{d_t}{\Delta T_s} = \frac{|d|\ cos\ (\alpha-\theta)}{\Delta T_s} \tag{6}$$

where $\theta = 8.2°$, and ΔS_s and ΔT_s are evaluated at the sample in which the solitary AF pixels were detected using the equations presented by *Giglio* [2013], reproduced from *Ichoku and Kaufman* [2005]. Note that the geometry in Figure 1 and the subtraction or addition of θ depend on the direction of the Terra or Aqua daytime or nighttime ground track.

The scalars $\hat{d}_s$ and $\hat{d}_t$ are unitless and indicate the relative amount of a ground footprint shared by two overlapping AF pixels detected in consecutive scans. For example, if $\hat{d}_s = 0.5$ and $\hat{d}_t = 0.0$, then AF_2 is displaced from AF_1 by one half the pixel dimension in the along-scan direction only. During selection of the AF pixels, $\hat{d}_s$ and $\hat{d}_t$ were limited to a maximum of 1.0. At a scan angle of 24°, the MODIS pixel geolocation accuracy goal of 50 m [*Wolfe et al.*, 2002] translates to a maximum error in the along-scan ($\delta\hat{d}_s$) and along-track ($\delta\hat{d}_t$)

direction of ±0.04 and ±0.05, respectively. As pixel sizes increase toward the scene edges, $\delta\hat{d}_s$ and $\delta\hat{d}_t$ decrease to ±0.01 and ±0.02, respectively. Therefore MODIS pixel geolocation errors are considered negligible for this analysis.

3.2. Clusters of Active Fire Pixels

Clusters of two AF pixels were analyzed similar to solitary AF pixels, but in equation (2), η was calculated using the two-pixel sum of FRP measured in the first scan, the two-pixel sum of FRP measured in the second scan, and their average. The use of the "bow-tie effect" to collect near-simultaneous measurements of the FRP emitted from clusters of three or more contiguous AF pixels, however, is compromised when larger clusters are only partially imaged in one or both scans. Instead, we propagate σ_η (in percent) by simulating 5000 aggregations ranging in size from 2 to 100 AF pixels. For each aggregation, (i) solitary AF pixels were randomly selected without replacement from those detected in the first scan only, (ii) the FRP was summed over all AF pixels composing the aggregation, (iii) the absolute uncertainty for each AF pixel (±MW) was calculated based upon ±1 σ_η determined for solitary pixels, (iv) the absolute uncertainty in the sum of FRP was calculated by summing in quadrature the absolute uncertainty for individual AF pixels, and (v) the relative uncertainty in the sum of FRP (in percent) was calculated by dividing the absolute uncertainty in the sum of FRP by the sum of FRP for the aggregation.

4. Results

More than 439,000 duplicated solitary AF pixels and 14,000 duplicated clusters of two AF pixels were detected globally by MODIS Terra and Aqua between 2003 and 2012. Duplicated AF pixels with overlapping ground footprints were detected at scan angles greater than 24°, and the minimum detectable FRP increased as a function of scan angle [*Freeborn et al.*, 2011; *Kumar et al.*, 2011], ranging from 8 MW at 30° to 44 MW at 55°. In the absence of the bow-tie effect, solitary AF pixels and clusters of two AF pixels accounted for 31% and 22% of the total number of AF pixels, and 16% and 15% of the summed FRP detected by MODIS at near-nadir scan angles less than 24°. Therefore, the following results represent a substantial proportion of the MOD14 and MYD14 records.

4.1. Solitary Active Fire Pixels

Results for solitary AF pixels detected by MODIS Terra indicate that η is approximately normally distributed with a mean (μ_η) of −0.2% and a standard deviation (σ_η) of 26.2%. Results are similar for MODIS Aqua ($\mu_\eta = -0.3\%$ and $\sigma_\eta = 26.8\%$). This is expected considering the large number of global multi-annual AF data and because the MODIS sensor is the same on both the Terra and Aqua satellites. Combining the MOD14 and MYD14 fire products yielded values of $\mu_\eta = -0.2\%$ and $\sigma_\eta = 26.6\%$ (Figure 2a). Henceforth, we present the combined results representative of both MODIS Terra and Aqua.

Whereas maximum scan-to-scan differences in T_f ($\Delta T_f = T_{f1} - T_{f2}$) approached ±50 K, scan-to-scan differences in the mean brightness temperature of the background window ($\Delta T_b = T_{b1} - T_{b2}$) did not exceed ±6 K. According to equations (3) and (4), these values translate to a standard deviation in η_f and η_b of $\sigma_f = 26.4\%$ and $\sigma_b = 4.1\%$, respectively. Hence, σ_η is overwhelmingly influenced by variability in the measurement of T_f rather than T_b. Although it is possible for ΔFRP to be entirely attributed to ΔT_b, this only occurs when η is small, i.e., within ±25%, or less than 1 σ_η (Figure 2b).

Whilst the true location of a fire with respect to any individual PSF remains unknown, the scan-to-scan displacement of AF_2 relative to AF_1 can be used to indicate the amount of ground footprint shared by the two PSFs. Sorting the duplicated solitary AF pixels according to $\hat{d}_s$ and $\hat{d}_t$ revealed that scan-to-scan differences in FRP are least variable ($\sigma_\eta = 11.1\%$) where the PSFs share the most overlap (i.e., where there is little scan-to-scan displacement between pixel centers), and scan-to-scan differences in FRP are more variable as AF_2 is displaced further from AF_1 (Figure 2c).

To elicit any dependence of σ_η on scan angle, duplicated solitary AF pixels were sorted according to $\hat{d}_s$ and $\hat{d}_t$. For observations with an equivalent amount of scan-to-scan overlap, there is no evidence that σ_η depends on scan angle (Figure 2d).

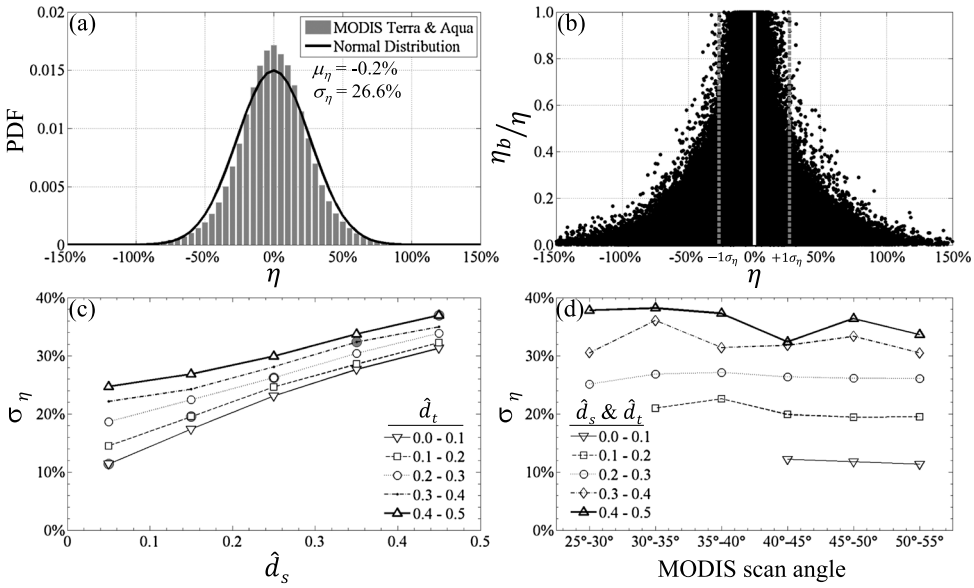

Figure 2. (a) Percent differences in FRP measured by MODIS Terra and Aqua in consecutive scans (η) are approximately normally distributed with a mean $\mu_\eta = -0.2\%$ and a standard deviation $\sigma_\eta = 26.6\%$. (b) Only when η is small is it possible for η to be entirely attributed to scan-to-scan differences in the mean brightness temperature of the background window (i.e., $\eta \cong \eta_b$ only if η is small). (c) Scan-to-scan variability in MODIS measurements of FRP (σ_η) increases with an increase in the relative along-track or along-scan pixel displacement, $\hat{d}_t$ and $\hat{d}_s$. (d) By comparing only solitary active fire pixels with an equivalent amount of scan-to-scan overlap in their point spread functions, there is no evidence that σ_η depends on scan angle.

4.2. Clusters of Active Fire Pixels

Results for MODIS Terra and Aqua indicate that $\sigma_\eta = 17.1\%$ for sums of FRP measured over clusters composed of two spatially adjacent AF pixels. In contrast to solitary AF pixels, where at least one adjacent along-scan pixel senses thermal radiance emitted by the fire but is not classified as an AF pixel, the omitted FRP adjacent to a solitary AF pixel is more likely be measured within a cluster of two contiguous along-scan AF pixels. Nevertheless, it is still possible for clusters of two AF pixels to respond differently—and to even subtend completely different sub-pixel combustion components—depending on the alignment of the fire within the PSFs.

Simulating larger aggregations is analogous to accumulating multiple AF pixels within an expanding spatial or temporal window (i.e., within a grid cell or within a MODIS compositing period). Large grid cells and long time periods include a multitude of AF pixels, each of which subtends different combustion components, which themselves will not be contiguous, nor from the same fire event, nor burning with the same reaction intensity due to local variations in fuel load, fuel condition, and wind speed. Propagating σ_η derived from solitary fire pixels indicates that for large aggregations, the relationship between the relative uncertainty in the sum of FRP and aggregation size (N) is well described using a power law (Figure 3). A value of $\sigma_\eta = 17.1\%$ for clusters of two AF pixels (obtained from direct observations above) is slightly less than a simulated value of $\sigma_\eta = 20.1\%$ obtained by aggregating two solitary AF pixels, perhaps suggesting a difference between "clusters" of contemporaneous, spatially adjacent AF pixels and "aggregations" of independent solitary AF pixels. As a conservative estimate, relative uncertainties in sums of FRP typically decrease to less than ~5% (based on $\pm 1\ \sigma_\eta$) for aggregations composed of more than ~50 MODIS AF pixels.

5. Discussion and Conclusions

Scan-to-scan differences in pixel brightness temperatures measured over large, thermally homogenous surfaces have been attributed to systematic errors and noise in the different MODIS detectors [*Liu et al.*, 2006; *Wenny et al.*, 2009]. In this application, however, since each MODIS AF pixel contains a hot target, scan-to-scan differences in FRP can be additionally attributed to (i) temporal variations in the true radiative output of the

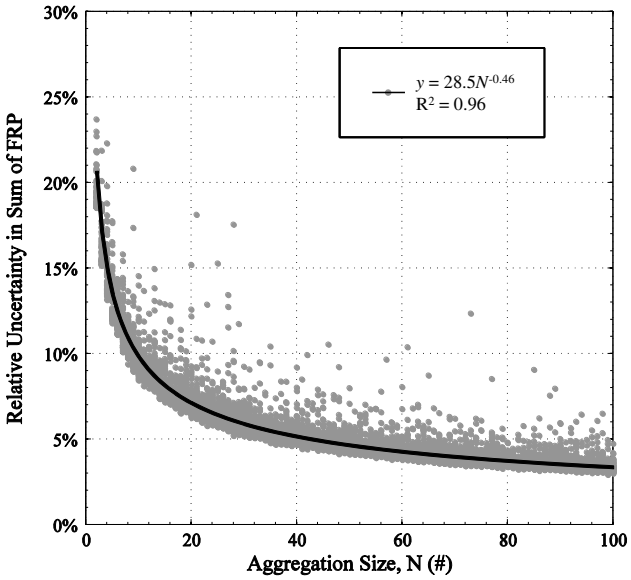

Figure 3. Relative uncertainty in the sum of FRP (in percent) measured by MODIS Terra and Aqua as a function of aggregation size (*N*). The relationship is based on a total of 5000 simulated aggregations composed of at least two randomly selected solitary active fire pixels, each assigned an uncertainty of ±1 σ_η (i.e., ±26.6%).

fire and the optical depth of the smoke plume, and (ii) scan-to-scan shifts of the fire within the imperfectly overlapping PSFs. With respect to the former, we argue that reaction intensities along different segments of the fireline may fluctuate independently such that if one flank flares up, another flank subsides, thus balancing the spatially integrated FRP emitted from the entire fire. We therefore assume that the true radiative output of the fire is invariant during the ~1.48 s between scans, and mainly attribute scan-to-scan differences in FRP to the displacement of the fire within the PSFs.

Given the large variability in MODIS measurements of FRP for individual AF pixels (±53.2% at the 95% confidence interval), we caution against interpreting FRP on a per-pixel basis without mapping the location of the fire within the MODIS PSF [e.g., *Peterson et al.*, 2013]. Nevertheless, for sufficiently large fires, or for sufficiently large spatiotemporal windows within which the AF pixels are accumulated, MODIS provides reliable measurements of the summed or average FRP, with uncertainties typically falling within ±7.0% (at ±2 σ_η) for aggregations composed of at least 100 AF pixels. Measurement uncertainties in FRP can be formally propagated if the data set contains per-pixel values (e.g., the MOD14/MYD14 products). Since the 8-day and monthly Climate Modeling Grid (CMG) products only contain the average FRP and the total number of AF pixels, the uncertainty budget for CMG grid cells can only be estimated using an assumed model (e.g., Figure 3). It should also be noted that whether MODIS provides accurate measurements of FRP remains to be evaluated.

Directly attaching uncertainties to MODIS measurements of FRP will enable more confident comparisons of active fire characteristics between fire regimes and through time. Furthermore, these uncertainties can be propagated to provide uncertainties in Earth system variables derived from MODIS measurements of FRP, such as biomass consumption, pyrogenic trace gas and aerosol production, and smoke plume heights. Although relatively large uncertainties in FRP limit confidence in the quantification fuel consumption rates and emission source strengths on a per-pixel basis, results presented in section 4.1 and Figure 3 indicate that the sensitivity of biomass burning estimates to FRP uncertainties can be mitigated by conducting inventories at increasingly coarser spatiotemporal resolutions. Regardless of scale, attaching uncertainties to pyrogenic parameters derived from FRP will permit more confident comparisons over space and time, and allow estimates to be more reliably compared with traditional bottom-up approaches.

Acknowledgments
M J Wooster was funded by the UK National Centre for Earth Observation, and the research leading to these results has received funding from the European Union's Seventh Framework Programme (FP7/2007–2013) under grant agreement 283576 (MACC-II project). The work of P.H.F and M.A.C. was supported by a NASA Interdisciplinary Sciences grant (NNX11AB89G). All authors would like to thank two anonymous reviewers and the editor for sharing their time and insight.

The Editor thanks two anonymous reviewers for assistance in evaluating this manuscript.

References

Barnes, W. L., T. S. Pagano, and V. V. Salomonson (1998), Pre-launch performance of the moderate resolution imaging spectroradiometer (MODIS) on EOS AM-1, *IEEE Trans. Geosci. Remote Sens.*, *36*(4), 1088–1100.

Bowman, D. M. J. S., et al. (2009), Fire in the Earth System, *Science*, *324*, 481–484, doi:10.1126/science.1163886.

Ellicott, E., E. Vermote, L. Giglio, and G. Roberts (2009), Estimating biomass consumed from fire using MODIS FRE, *Geophys. Res. Lett.*, *36*, L13401, doi:10.1029/2009GL038581.

Freeborn, P. H., M. J. Wooster, and G. Roberts (2011), Addressing the spatiotemporal sampling design of MODIS to provide estimates of the fire radiative energy emitted from Africa, *Remote Sens. Environ.*, *115*(2), 475–489, doi:10.1016/j.rse.2010.09.017.

Giglio, L. (2013), MODIS Collection 5 Active Fire Product User's Guide, Version 2.5, 61 pp., Dep. of Geogr., Univ. of Maryland, College Park, Md.

Giglio, L., J. Descloitres, C. O. Justice, and Y. Kaufman (2003), An enhanced contextual fire detection algorithm for MODIS, *Remote Sens. Environ.*, *87*, 273–282.

Ichoku, C., and Y. J. Kaufman (2005), A method to derive smoke emission rates from MODIS fire radiative energy measurements, *IEEE Trans. Geosci. Remote Sens.*, *43*(11), 2636–2649, doi:10.1109/TGRS.2005.857328.

Ichoku, C., L. Giglio, M. J. Wooster, and L. A. Remer (2008), Global characterization of biomass-burning patterns using satellite measurements of fire radiative energy, *Remote Sens. Environ.*, *112*, 2950–2962.

Kaiser, J. W., et al. (2012), Biomass burning emissions estimated with a global fire assimilation system based on observations of fire radiative power, *Biogeosciences*, *9*, 527–554, doi:10.5194/bg-9-527-2012.

Kaufman, Y. J., L. A. Remer, R. D. Ottmar, D. E. Ward, R. R. Li, R. Kleidman, R. S. Fraser, L. P. Flynn, D. McDougal, and G. Shelton (1996), Relationship between remotely sensed fire intensity and rate of emission of smoke: SCAR-C Experiment, in *Global Biomass Burning*, edited by J. Levine, pp. 685–696 , MIT Press, Cambridge, Mass.

Kaufman, Y. J., C. O. Justice, L. P. Flynn, J. D. Kendall, E. M. Prins, L. Giglio, D. E. Ward, W. P. Menzel, and A. W. Setzer (1998), Potential global fire monitoring from EOS-MODIS, *J. Geophys. Res.*, *103*(D24), 32,215–32,338.

Kumar, S. S., D. P. Roy, L. Boschetti, and R. Kremens (2011), Exploiting the power law distribution properties of satellite fire radiative power retrievals - a method to estimate fire radiative energy and biomass burned from sparse satellite observations, *J. Geophys. Res.*, *116*, D19303, doi:10.1029/2011JD015676.

Liu, R. G., J. Y. Liu, and S. Liang (2006), Estimation of Systematic Errors in MODIS Thermal Infrared Bands, *IEEE Geosci. Remote Sens. Lett.*, *3*(4), 541–545.

Mazzoni, D., J. A. Logan, D. Diner, R. Kahn, L. Tong, and Q. Li (2007), A data-mining approach to associating MISR smoke plume heights with MODIS fire measurements, *Remote Sens. Environ.*, *107*, 138–148, doi:10.1016/j.rse.2006.08.014.

Nishihama, M., R. Wolfe, D. Solomon, F. Patt, J. Blanchette, A. Fleig, and E. Masuoka (1997), MODIS level 1A Earth location: Algorithm theoretical basis document version 3.0, MODIS Science Data Support Team, NASA Goddard Space Flight Center, Greenbelt, Md.

Peterson, D., J. Wang, C. M. Ichoku, E. Hyer, and V. Ambrosia (2013), A sub-pixel-based calculation of fire radiative power from MODIS observations: 1 Algorithm development and initial assessment, *Remote Sens. Environ.*, *129*, 262–279, doi:10.1016/j.rse.2012.10.036.

Roberts, G. J., and M. J. Wooster (2008), Fire detection and fire characterization over Africa using Meteosat SEVIRI, *IEEE Trans. Geosci. Remote Sens.*, *46*(4), 1200–1218.

Schroeder, W., I. Csiszar, L. Giglio, and C. C. Schmidt (2010), On the use of fire radiative power, area, and temperature estimates to characterize biomass burning via moderate to coarse spatial resolution remote sensing data in the Brazilian Amazon, *J. Geophys. Res.*, *115*, D21121, doi:10.1029/2009JD013769.

Seiler, W., and P. J. Crutzen (1980), Estimates of gross and net fluxes of carbon between the biosphere and the atmosphere form biomass burning, *Clim. Change*, *2*, 207–247.

Smith, A. M. S., and M. J. Wooster (2005), Remote classification of head and backfire types from MODIS fire radiative power observations, *Int. J. Wildland Fire*, *14*, 249–254.

Val Martin, M., J. A. Logan, R. A. Kahn, F.-Y. Leung, D. L. Nelson, and D. J. Diner (2010), Smoke injection heights from fires in North America: Analysis of 5 years of satellite observations, *Atmos. Chem. Phys.*, *10*, 1491–1510, doi:10.5194/acp-10-1491-2010.

Vermote, E., E. Ellicott, O. Dubovik, T. Lapyonok, M. Chin, L. Giglio, and G. J. Roberts (2009), An approach to estimate global biomass burning emissions of organic and black carbon from MODIS fire radiative power, *J. Geophys. Res.*, *114*, D18205, doi:10.1029/2008JD011188.

Wenny, B. N., X. Geng, and X. Xiong (2009), MODIS thermal emissive band detector bias, in *Proceedings of SPIE on Sensors, Systems, and Next-Generation Satellites XIII*, vol. 7474, edited by R. Meynart, S. P. Neeck, and H. Shimoda, pp. 74740V-1-10, SPIE, Bellingham, Wash., doi:10.1117/12.830080.

Wolfe, R., M. Nishihama, A. Fleig, J. Kuyper, D. Roy, J. Storey, and F. Patt (2002), Achieving sub-pixel geolocation accuracy in support of MODIS land science, *Remote Sens. Environ.*, *83*, 31–49.

Wooster, M. J., and Y.-H. Zhang (2004), Boreal forest fires burn less intensely in Russia than in North America, *Geophys. Res. Lett.*, *31*, L20505, doi:10.1029/2004GL020805.

Wooster, M. J., B. Zhukov, and D. Oertel (2003), Fire radiative energy for quantitative study of biomass burning: Derivation from the BIRD experimental satellite and comparison to MODIS fire products, *Remote Sens. Environ.*, *86*(1), 83–107.

Xu, W., M. J. Wooster, G. Roberts, and P. Freeborn (2010), New GOES imager algorithms for cloud and active fire detection and fire radiative power assessment across North, South and Central America, *Remote Sens. Environ.*, *114*(9), 1876–1895, doi:10.1016/j.rse.2010.03.012.